Materials Transactions, Vol. 46, No. 12 (2005) pp. 2954 to 2958
Special Issue on Materials Science of Bulk Metallic Glasses

Mechanical Behavior of $Zr_{65}Al_{10}Ni_{10}Cu_{15}$ and $Zr_{52.5}Al_{10}Ni_{10}Cu_{15}Be_{12.5}$ Bulk Metallic Glasses

Weihuo Li[1,2], Bingchen Wei[2,*], Taihua Zhang[3], Lingchen Zhang[2] and Yuanda Dong[1]

[1]*Institute of Materials, Shanghai University, Shanghai 200072, P. R. China*
[2]*National Microgravity Laboratory, Institute of Mechanics, Chinese Academy of Sciences, Beijing 100080, P. R. China*
[3]*State Key Laboratory of Nonlinear Mechanics (LNM), Institute of Mechanics, Chinese Academy of Sciences, Beijing 100080, P. R. China*

The thermal stability and the mechanical behavior of $Zr_{65}Al_{10}Ni_{10}Cu_{15}$ and $Zr_{52.5}Al_{10}Ni_{10}Cu_{15}Be_{12.5}$ bulk metallic glasses (BMGs) were investigated by differential scanning calorimetry, uniaxial compressive test, ultrasonic method, and nanoindentation. The substitution of Zr by Be significantly improved the thermal stability of the amorphous phase, exhibited by a wide supercooled liquid region of 116 K. The Be containing BMG exhibited a compressive strength of 1780 MPa, and in particular a high plastic strain of about 6%. The simultaneous operation of multiple shear bands during plastic deformation in $Zr_{52.5}Al_{10}Ni_{10}Cu_{15}Be_{12.5}$ BMG is proved by the less pronounced serrated flow during the loading process in the compression and nanoindentation, as well as the fracture surface morphologies. A high Debye temperature derived from the ultrasonic measurements indicates a condensed atomic arrangement in the Be containing BMG, and may responsible for the high thermal stability.

(Received June 20, 2005; Accepted August 30, 2005; Published December 15, 2005)

Keywords: *bulk metallic glass, mechanical property, shear band, nanoindentation*

1. Introduction

Bulk metallic glasses (BMGs) have been highly attracted as a new structural material in recent years due to their excellent mechanical properties, such as high strength, good wear resistance, excellent elasticity and easily forming in viscous state.[1–4] However, it is well known from earlier work that plastic deformation in metallic glasses is concentrated into narrow regions called shear bands at room temperature. The less macroscopic plastic deformability has limited the applications of BMGs as engineering materials. Therefore, considerable efforts have been made to explore ductile bulk metallic glasses in recent years.[5–7] Multi-component Zr-based BMGs have been widely investigated.[4,8–12] These alloys can be prepared at low cooling rates and usually have wide supercooled regions. However, detailed studies on the deformation mechanisms of monolithic metallic glasses is still limited, because of the typically poor plastic flow (0–2% under uniaxial compression) at room temperature.[10,11]

In the present work, $Zr_{52.5}Al_{10}Ni_{10}Cu_{15}Be_{12.5}$ BMG with a high compressive plastic strain of 6% is reported. The deformation behavior of the BMG is compared with that of $Zr_{65}Al_{10}Ni_{10}Cu_{15}$ BMG through uniaxial compressive test, nanoindentation, and ultrasonic measurement.

2. Experimental Procedures

Cylinder rods with 5 mm in diameter of $Zr_{65}Al_{10}Ni_{10}Cu_{15}$ and $Zr_{52.5}Al_{10}Ni_{10}Cu_{15}Be_{12.5}$ BMGs were prepared by melting pure metals in an argon atmosphere and then suction-casting in a copper mould. The structure of samples was characterized by X-ray diffraction (XRD) in a Philips PW 1050 diffractometer using Cu K_α radiation. Thermal analysis was performed with a Perkin-Elmer DSC-7 differential scanning calorimeter under argon atmosphere. A constant heating rate of 0.33 K/s was employed. The acoustic velocities were measured by a pulse echo overlap method using a MATEC 6600 ultrasonic system with a 10 MHz frequency.[13,14] The density was measured by the Archimedean technique and the accuracy is 0.1%. Elastic constants (*e.g.*, Young's modulus E, shear modulus G, bulk modulus B, and Poisson's ratio) and Debye temperature θ of the BMGs were derived from the acoustic velocities and densities. The uniaxial compressive tests on cylindrical samples of 3 mm in diameter and 6 mm in length were performed in a commercial Instron-type testing machine at room temperature. The cross-head was moved at a constant speed with an initial strain rate of $1.0 \times 10^{-4}\ s^{-1}$. The specimens for nanoindentation measurements were mechanically polished to a mirror finish and tested in a MTS Nano Indenter® XP with a Berkovich diamond tip. A fused silica was used as a standard sample for the initial calibration. The indentations were performed in load-control mode to a depth limit of 1 μm using loading rates of 0.5 mN/s. The thermal drift of the instrument was maintained below 0.05 nm/s. At least six indentations were made for each test on each specimen. All tests were carried out at 23°C. The compressive fracture surface and nano-indention surface observations were performed by a JSM-6460 scanning electron microscope (SEM).

3. Results and Discussion

Figure 1 shows the XRD patterns of as-cast $Zr_{65}Al_{10}Ni_{10}Cu_{15}$ and $Zr_{52.5}Al_{10}Ni_{10}Cu_{15}Be_{12.5}$ samples. All as-cast alloys exhibit XRD spectrum typical for amorphous phase without obvious crystalline peak. Figure 2 shows the DSC traces of the $Zr_{65}Al_{10}Ni_{10}Cu_{15}$ and $Zr_{52.5}Al_{10}Ni_{10}Cu_{15}Be_{12.5}$ alloys at a constant scanning rate of 0.33 K/s. The onset temperature of the glass transition (T_g), the crystallization temperature (T_x) and supercooled liquid region ($\Delta T_x =$

*Corresponding author, E-mail: weibc@imech.ac.cn

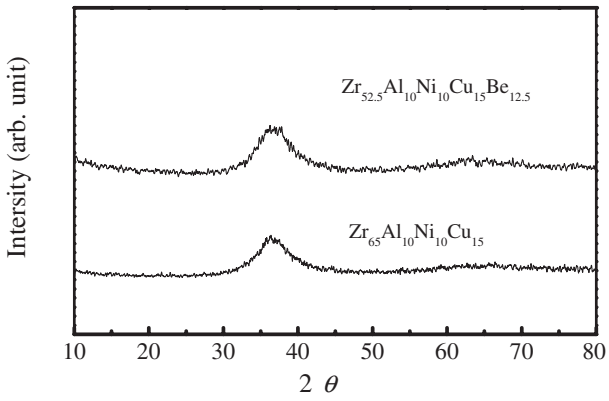

Fig. 1 XRD patterns for $Zr_{65}Al_{10}Ni_{10}Cu_{15}$ and $Zr_{52.5}Al_{10}Ni_{10}Cu_{15}Be_{12.5}$ BMGs.

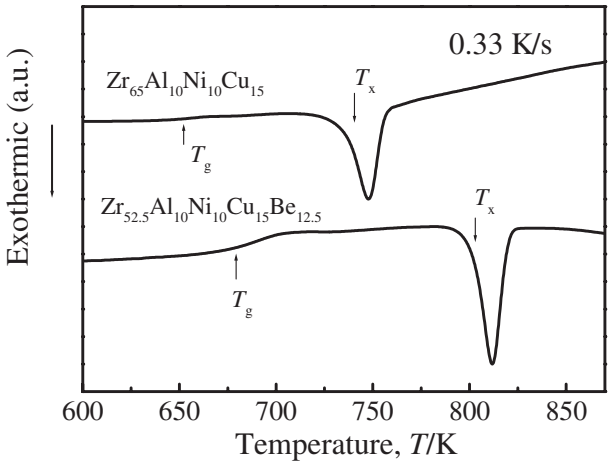

Fig. 2 DSC curves of $Zr_{65}Al_{10}Ni_{10}Cu_{15}$ and $Zr_{52.5}Al_{10}Ni_{10}Cu_{15}Be_{12.5}$ BMGs at the heating rate of 0.33 K/s.

$T_x - T_g$) are 652, 734, and 82 K, respectively for the Be free BMG. The Be containing BMG exhibits higher T_g and T_x values, and a wide ΔT_x of 116 K. The reduced glass transition temperature ($T_{rg} = T_g/T_l$, where T_l is the liquidus temperature) is 0.58 and 0.70 for the Be free and Be containing BMG, respectively. The T_x and ΔT_x values for the present two BMGs are slightly lower than the data in Ref. 15), which is measured at a higher heating rate. The slight difference should be caused by the kinetic effect of the crystallization process. The quite wide ΔT_x and high T_{rg} value for $Zr_{52.5}Al_{10}Ni_{10}Cu_{15}Be_{12.5}$ indicate the thermal stability and glass forming ability are greatly improved by substituting Be for Zr.

Figure 3 shows the stress–strain curves of $Zr_{65}Al_{10}Ni_{10}Cu_{15}$ and $Zr_{52.5}Al_{10}Ni_{10}Cu_{15}Be_{12.5}$ BMGs measured under the initial strain rate of $1.0 \times 10^{-4}\,s^{-1}$ at room temperature. It is well known that a high strain rate promotes the inhomogeneous plastic deformation in BMGs, which is characterized by the formation of strongly localized shear bands, followed by catastrophic fracture. A relatively low strain rate is employed in the present tests for the detailed study of the plastic deformation process in the two BMGs. The Be free BMG exhibits a elastic modulus of 81.3 GPa and elastic limit of about 2.0% followed by a distinct plastic flow

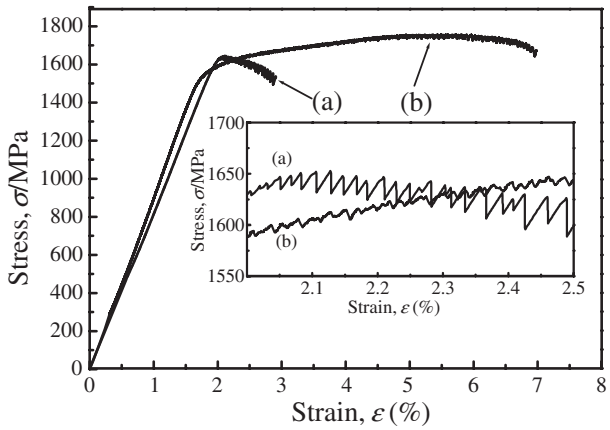

Fig. 3 Stress–Strain curves of (a) $Zr_{65}Al_{10}Ni_{10}Cu_{15}$ and (b) $Zr_{52.5}Al_{10}Ni_{10}Cu_{15}Be_{12.5}$ BMGs under compression at the strain rate of $1.0 \times 10^{-4}\,s^{-1}$. The inset shows serrated flow phenomenon on an enlarged scale.

with yielding strength (σ_y) of 1650 MPa, and then final fail with the compressive fracture strain of about 1%. These compressive properties and work softening phenomenon are in agreement with the results of BMGs with similar chemical composition.[16] The Be containing BMG exhibits a elastic modulus of 92.7 GPa, elastic limit of 1.7%, yield strength of 1525 MPa, and in particular a large compressive fracture strain of about 6%. Moreover, it is very clear that there is an increase of the flow stress after yielding in the Be containing BMG. The increase in the flow stress was measured to be from 1525 to 1780 MPa from the true stress-strain diagram. It should also be noted that a significant serration flow was revealed during the plastic deformation in the two BMGs. The inset of Fig. 3 highlights the serration behavior in two BMGs. The stress and strain (or time) magnitudes of each serration in the Be free BMG are much larger than that of Be containing BMG. At the same plastic strain, *e.g.* 0.5%, the stress magnitude is about 30 MPa for the Be free BMG, and 10 MPa for the Be containing BMG. The average stress magnitude of each serration is about 30 MPa for the Be free BMG, while 10 MPa for the Be containing BMG.

It is widely accepted that each serration on the stress–strain curves corresponds to the activation of single shear bands.[17] Compared with the Be free BMG, the Be containing BMG exhibits a much smaller magnitude and a much larger number of serrations during the plastic flow. This indicates that multiple shear bands are activated during the plastic deformation in the Be containing alloy, and the propagation of single shear bands is suppressed. The sample surface and fracture surface of the two BMGs after uniaxial compressive tests are shown in Fig. 4. For $Zr_{65}Al_{10}Ni_{10}Cu_{15}$ BMG, a few shear bands can be observed at an angle of about 45° with respect to the stress axis and paralleled to the fracture plane in Fig. 4(a). The fracture surface consists of vein-like pattern and featureless regions [Fig. 4(b)]. While in the $Zr_{52.5}Al_{10}Ni_{10}Cu_{15}Be_{12.5}$ BMG, intersected multiple shear bands with a smaller upset size can be observed on the sample surface [Fig. 4(c)]. Well-developed vein-like pattern can be seen on the fracture surface [Fig. 4(d)], and the size of veins is smaller than that in the former BMG. The observation on the fracture morphology confirms the activa-

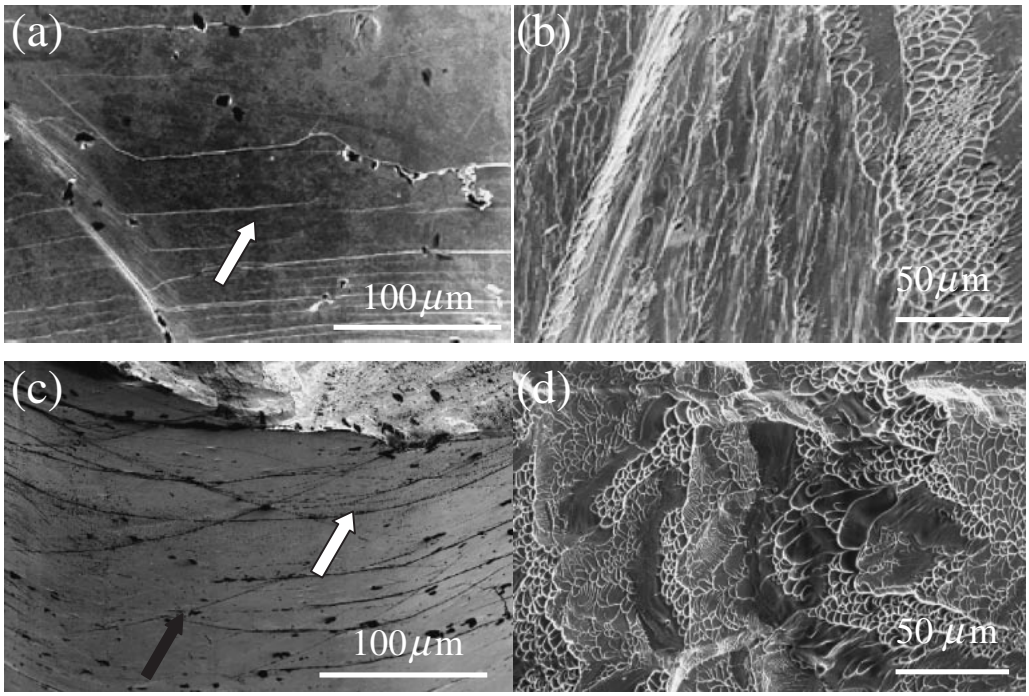

Fig. 4 SEM images of the fracture surfaces of $Zr_{65}Al_{10}Ni_{10}Cu_{15}$ (a, b) and $Zr_{52.5}Al_{10}Ni_{10}Cu_{15}Be_{12.5}$(c, d) at the strain rate of $1.4 \times 10^{-4}\,s^{-1}$. Primary shear bands were marked with white arrows, and secondary bands with black arrows.

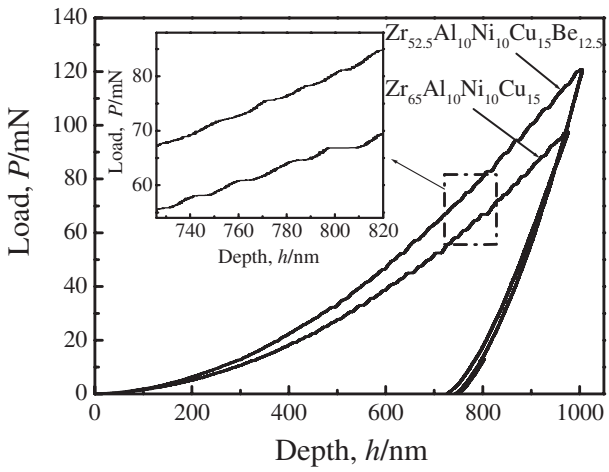

Fig. 5 Typical load–depth (P–h) curves during nanoindentations at the loading rate 0.1 mN/s for both BMGs. The inset shows serrated flow phenomenon on an enlarged scale.

tion of multiple shear bands before final fracture in the Be containing BMG. In order to further investigate the deformation behavior of the two BMGs, nanoindentation measurements were conducted.

Figure 5 shows the load–depth (P–h) curves of the two BMGs at the loading rate of 0.1 mN/s. The inset exhibits the enlarged parts of the P–h curves. The hardness and elastic modulus of both BMGs are obtained from the nanoindnetation curves using Oliver–Pharr method.[18] The hardness (H) and elastic modulus of $Zr_{65}Al_{10}Ni_{10}Cu_{15}$ BMG are 5.67 and 109.8 GPa, respectively, and the corresponding values for $Zr_{52.5}Al_{10}Ni_{10}Cu_{15}Be_{12.5}$ BMG are 6.87 and 128.3 GPa, respectively. The ratio of H/σ_y is 3.44 for the former BMG, and 4.50 for the later BMG. The elastic modulus determined from the nanoindentation measurements is larger than that from compressive tests by 28 and 26% for the Be free BMG and Be containing BMG, respectively. The higher modulus values in the nanoindention measurements may be caused by the pile-up effect around the indents. Distinct serrated flow can be observed in the loading portion of the Be free BMG. The load–depth (P–h) curve is punctuated by discrete steps with the size increasing gradually with the penetration depth. This phenomenon is in agreement with the nanoindentation results of the BMG with the same chemical composition.[19] The selected loading rate in the present measurements is in the loading rate range, where serrated flow can be easily observed on the loading part of P–h curves.[19] Whereas, much less pronounced serrated flow is revealed in the Be containing BMG during the loading process at the same indentation loading rate. The discrete steps in the loading curve of nanoindentation were also ascribed to the activation of single shear bands during plastic deformation.[19–22] The much larger size of each step in the Be free BMG further confirms that the easy propagation of a single shear band. While, in the Be containing BMG, the propagation of a single shear band is suppressed, and the simultaneous operation of multiple shear bands contributes to the relative homogeneous plastic deformation.

Typical surface morphologies of indents for the two BMGs after indentation measurements are shown in Fig. 6. A number of significant incomplete circular patterns of shear bands were observed in the pile-up area around the indents for $Zr_{65}Al_{10}Ni_{10}Cu_{15}$ BMG [Fig. 6(a)]. They represent overlapping layers of displaced material that flow upwards and away from the depth of the indents. $Zr_{52.5}Al_{10}Ni_{10}Cu_{15}Be_{12.5}$ BMG also exhibits shear bands pattern surrounding the indents [Fig. 6(b)]. The number of shear bands is larger than

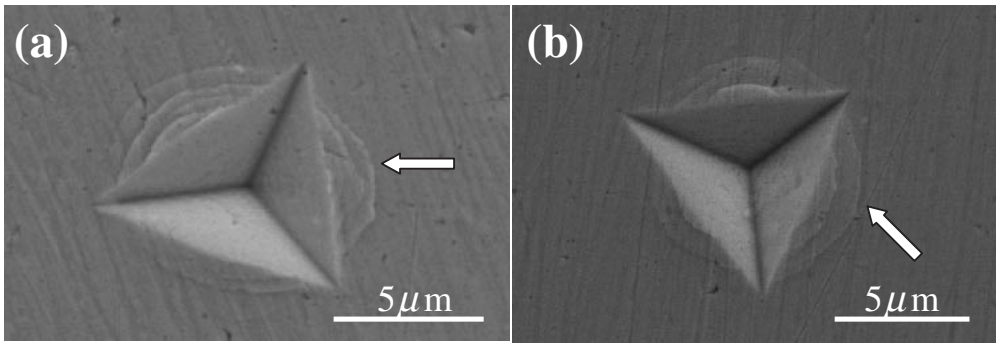

Fig. 6 SEM images of the evolved deformation features after indentation at 1000 nm depth for both BMGs: (a) $Zr_{65}Al_{10}Ni_{10}Cu_{15}$ and (b) $Zr_{52.5}Al_{10}Ni_{10}Cu_{15}Be_{12.5}$. The localized plastic flow as marked with arrows.

Table 1 Elastic constants for amorphous $Zr_{65}Al_{10}Ni_{10}Cu_{15}$, $Zr_{52.5}Al_{10}Ni_{10}Cu_{15}Be_{12.5}$ and $Zr_{41}Ti_{14}Cu_{12.5}Ni_{10}Be_{22.5}$ calculated from ultrasonic measurements of the transverse speed, v_s, and longitudinal speed of sound v_l. G denotes the shear modulus, E Young's modulus, B the bulk modulus, ρ the alloy's density, θ the Debye temperature and ν Poisson's ratio.

Alloys	v_l (Km/s)	v_s (Km/s)	ρ (g/cm^3)	B (GPa)	E (GPa)	G (GPa)	θ (K)	ν
$Zr_{65}Al_{10}Ni_{10}Cu_{15}$	4.814	2.139	6.612	113.0	82.3	30.3	324	0.377
$Zr_{52.5}Al_{10}Ni_{10}Cu_{15}Be_{12.5}$	4.994	2.364	6.316	110.5	95.7	35.3	371	0.356
$Zr_{41}Ti_{14}Cu_{12.5}Ni_{10}Be_{22.5}$*	5.174	2.472	6.125	114.1	101.2	37.4	327	0.352

*Data taken from Ref. 14)

that in the Be free BMG, and the upset height of shear bands is much smaller that that in the former BMG. This proves that the operation of multiple shear bands with relatively small thickness during plastic deformation, which leads to a smoother pile-up region around the indents with less pronounced shear band upsets.

The study on the plastic deformation behavior of compression and nanoindentation tests proves the simultaneous operation of multiple shear bands in the $Zr_{52.5}Al_{10}Ni_{10}Cu_{15}Be_{12.5}$ BMG during plastic deformation. This should be the reason for the attractive large compressive fracture strain. The local atomic arrangements and compositions near the shear bands play an important role in the formation and propagation of shear bands. In order to further understand the mechanical properties, ultrasonic measurements were carried out to determine the sound velocity in the two BMGs. Elastic constants were calculated from the sound velocities and are shown in Table 1. The values for $Zr_{41}Ti_{14}Cu_{12.5}Ni_{10}Be_{22.5}$ BMG are also presented for comparison. Both the transverse speed of sound (v_t) and the longitudinal speed of sound (v_l) increase with the substitution of Zr by Be. The shear modulus (G) and bulk modulus (B) exhibited the same tendency. The ratio of G/B is 0.27 for $Zr_{65}Al_{10}Ni_{10}Cu_{15}$ BMG, and 0.32 for $Zr_{52.5}Al_{10}Ni_{10}Cu_{15}Be_{12.5}$BMG. Moreover, the Poisson's ratio (ν) is 0.377 for the former BMG, and 0.356 for the later BMG. The $Zr_{52.5}Al_{10}Ni_{10}Cu_{15}Be_{12.5}$BMG exhibits a high compressive fracture strain, but it possesses a higher ratio of G/B and a lower value of ν. This is in contrast with the results of $Pt_{57.5}Cu_{14.7}Ni_{5.3}P_{22.5}$ BMG, for which the high ductility is ascribed to a low G/K ratio and a high ν value.[23] The Debye temperature (θ) of $Zr_{52.5}Al_{10}Ni_{10}Cu_{15}Be_{12.5}$BMG has larger values than that of $Zr_{65}Al_{10}Ni_{10}Cu_{15}$ BMG. This suggests a condensed local atomic arrangement with the addition of 12.5%Be. The condensed atomic packing is also responsible for the high thermal stability in this BMG with a quite wide supercooled liquid region.

4. Conclusions

In conclusion, bulk amorphous alloys with good glass-forming ability for $Zr_{65}Al_{10}Ni_{10}Cu_{15}$ and $Zr_{52.5}Al_{10}Ni_{10}Cu_{15}Be_{12.5}$ have been prepared by copper mould casting. Addition of 12.5 at%Be to the $Zr_{65}Al_{10}Ni_{10}Cu_{15}$ BMG enhances the thermal stability of the amorphous phase and improves the compressive fracture strain significantly. The simultaneous operation of multiple shear bands in the $Zr_{52.5}Al_{10}Ni_{10}Cu_{15}Be_{12.5}$ BMG is responsible for the weak serrated flow in compression and nanoindentation tests, thereby contribute to the good ductility.

Acknowledgements

The authors would like to acknowledge the financial support provided by National Nature Science Foundation of China (Grant Nos. 50571109, 10372103 and 10432050) and the Knowledge Innovation Program of Chinese Academy of Sciences.

REFERENCES

1) A. Inoue: Mater. Trans., JIM **36** (1995) 866–875.
2) A. Inoue: Acta Mater. **28** (2000) 279–306.
3) W. L. Johnson: MRS Bulletin **24** (1999) 42–56.
4) A. Peker and W. L. Johnson: Appl. Phys. Lett. **63** (1993) 2342–2344.
5) H. Choi-Yim and W. L. Johnson: Appl. Phys. Lett. **71** (1997) 3808–3810.
6) C. Fan, D. V. Louzguine, C. F. Li and A. Inoue: Appl. Phys. Lett. **75** (1999) 341–343.
7) L. Q. Xing, Y. Li, K. T. Ramesh, J. Li and T. C. Hufngel: Phy. Rev. B

64 (2001) 180201–180204.
8) A. Inoue, T. Zhang, N. Nishiyama, K. Ohba and T. Masumato: Mater. Trans., JIM **34** (1993) 1234–1237.
9) A. Inoue, T. Zhang and T. Masumoto: Mater. Trans., JIM **31** (1990) 177–183.
10) H. Kato, Y. Kawamure and A. Inoue: Mater. Trans., JIM **37** (1996) 70–77.
11) L. F. Liu, L. H. Dai, Y. L. Bai, B. C. Wei and J. Eckert: Mater. Chem. Phys. **93** (2005) 174–177.
12) Y. Zhang, M. X. Pang, D. Q. Zhao, R. J. Wang and W. H. Wang: Mater. Trans., JIM **11** (2000) 1410–1414.
13) L. M. Wang, W. H. Wang, R. J. Wang, Z. J. Zang, D. Y. Dai and L. L. Sun: Appl. Phys. Lett. **77** (2002) 1147–1149.
14) W. H. Wang, L. L. Li, M. X. Pan and R. J. Wang: Phys. Rev. B **63** (2001) 052204–052207.
15) X. S. Xiao, S. S. Fang, L. Xia, W. H. Li, Q. Hua and Y. D. Dong: J. Alloys Compd. **351** (2003) 324–328.
16) Y. Kawamura, T. Shibata, A. Inoue and T. Masumoto: Appl. Phys. Lett. **69** (1996) 1208–1210.
17) F. Spacepen: Acta Metall. **25** (1977) 407–415.
18) W. C. Oliver and G. M. Pharr: J. Mater. Res. **7** (1992) 1564–1583.
19) C. A. Schuh and T. G. Nieh: Acta Mater. **51** (2003) 87–99.
20) T. G. Nieh, C. Schuh, J. Wadsworth and Y. Li: Intermetallics **10** (2002) 1177–1182.
21) W. H. Jiang and M. Atzmon: J. Mater. Res. **18** (2003) 755–757.
22) B. C. Wei, T. H. Zhang, W. H. Li, Y. F. Sun, Y. Yu and Y. R. Wang: Intermetallics **12** (2004) 1239–1243.
23) J. Schroers and W. L. Johnson: Phys. Rev. Lett. **93** (2004) 155506–155509.